Investigation of flow and turbulence in carotid artery models of varying compliance using particle image velocimetry

A.L. DiCarlo[1] and T. Poepping[1]

[1] Department of Physics and Astronomy, University of Western Ontario, London, Canada

Abstract— **Atherosclerosis in the carotid artery is one of the main risk factors for stroke. Arterial compliance, a measure of the elasticity of blood vessels, is a common indicator of vascular disease and is known to decrease in association with other stroke risk factors, including age, diabetes, and hypertension. Decreased local compliance leads to changes in the flow and pressure waveforms and corresponding changes in the velocity field. Resulting hemodynamic parameters, such as shear stress and turbulence, play a primary role in the process of plaque and clot formation. The aim of this work was to analyze the effect of compliance on carotid artery flow patterns and turbulence intensity experimentally within carotid artery phantoms. This was accomplished using Particle image velocimetry (PIV), an established engineering technique for measuring velocity fields with high temporal and spatial resolution that can be applied to study specific aspects of the flow system when used in controlled test models. Results showed slightly higher overall velocities in rigid phantoms compared to geometrically-matched compliant versions. A stiffer vessel wall resulted in increased maximum average turbulence intensities, 0.41±0.02 m/s in compliant models and 0.48±0.03 m/s in rigid phantom models. The rigid vessel region of maximum turbulence also occurred more upstream compared to the bifurcation apex.**

Keywords— **Particle image velocimetry, carotid artery, hemodynamics, stroke, atherosclerosis**

I. Introduction

Stroke and cardiovascular disease are one of the leading causes of death and morbidity worldwide. The carotid bifurcation is a common site of atherosclerosis. Atherosclerosis can lead to thrombus formation and subsequently, stroke. The process of thrombus formation is not only driven by the presence of chemical agonists in the blood, but also by complex hemodynamics and changes in flow which commonly arise at sites of plaque development. [10] These altered flow patterns, including increased turbulence, high shear gradients, and low oscillatory shear stress, can promote further development of plaque and subsequently plaque rupture and thromboembolism

Disturbed flow conditions, such as those seen at stenoses, have been shown to be correlated with increased thrombus production related to an increase in the measured turbulence intensity [15]. In addition, plaque rupture has been shown to be localized to high shear stress regions [3].

Arterial compliance decreases in conjunction with the presence of a number of known cardiovascular risk factors – including age, hypertension, and diabetes [1] – and is associated with atherosclerosis at various sites in the arterial tree [18]. Furthermore, arterial compliance has been shown to be an independent predictor of ischemic stroke risk, transient ischemic attack, and even fatal stroke events [2,9,16,17], separate from additional cardiovascular risk factors.

Particle Image Velocimetry (PIV) is a standard optical engineering laboratory technique used to study complex flows and is favourable due to the ability to achieve high temporal and spatial resolution. Previously, we have shown the effects of stenosis severity, plaque eccentricity and ulceration on local hemodynamics within the carotid bifurcation using a custom in vitro flow facility [7,8]. The present work aims to characterize the effect of carotid artery compliance on local hemodynamics using PIV.

II. Methods

A. Flow Set-up

Life-sized carotid artery bifurcation models with 8 mm common carotid artery (CCA) diameter and 50% eccentric stenosis of the internal carotid artery (ICA) were fabricated from transparent polydimethylsiloxane (PDMS) Sylgard 184 (elastic modulus 1.3 MPa) [11,14]. Semi-compliant and rigid versions with identical vessel geometry allow the effects of distensibility to be investigated. The essentially rigid phantom was constructed as a silicone block model (i.e. large wall thickness with undetectable wall motion). A more compliant version was achieved by using a thin-walled vessel with approximate 1-mm wall thickness, suspended in a transparent box surrounded by index-matched fluid for optical viewing. Phantoms were perfused with a refractive-index matched blood-mimicking fluid (n = 1.4140) with dynamic viscosity in the range of human blood (μ = 4.31cP) [20]. The density of the fluid was 1.244g/mL, in the physiological range and also approximating the density of polystyrene, fluorescent microspheres used as tracer particles. Fluid was circulated through a flow loop using a

D.A. Jaffray (ed.), *World Congress on Medical Physics and Biomedical Engineering, June 7-12, 2015, Toronto, Canada*,
IFMBE Proceedings 51, DOI: 10.1007/978-3-319-19387-8_423

computer controlled positive displacement pump [5] generating a physiological pulsatile flow waveform previously characterized [6]. In addition, the flow loop contained electromagnetic flow meters at the CCA inlet and internal (ICA) and external (ECA) outlets, as well as downstream flow resistors consisting of small diameter tubing to achieve approximately a 60:30 ICA:ECA flow division. [4,11]. Peak and mean flow rates measured at the CCA entrance were 23.3±0.1 mL/s and 6.4±0.1 mL/s respectively.

B. Data Acquisition and Analysis

PIV data acquisition was completed using a stereoscopic PIV system previously described [7]. The laser sheet was collimated to 1 mm thick in the region of interest. High speed cameras were equipped with low-pass filters to eliminate reflections and isolate signal from tracer particles. Volumetric data was acquired by adjusting the elevation of the phantom in 0.5 mm increments for a total of 15 horizontal planes. Thirty cardiac cycles were collected for each plane.

The acquisition was synchronized via an external trigger signal generated by the pump. Double-frame exposure PIV images were collected at a frame rate of 100Hz for the first 870 ms of each 920 ms cardiac cycle (neglecting a portion of nearly constant flow during end diastole to ensure capturing consecutive cardiac cycles).

A root mean square mask was applied to raw particle images prior to velocity computation to eliminate non-flow regions. Unique masks were created for each cardiac cycle time point and plane to account for possible wall motion in semi-compliant model. Velocity vectors were computed using DaVis software (LaVision, Inc.) using a fast-fourier transform cross correlation multipass algorithm with decreasing window size from 64x64 pixels to 16x16 pixels with 50% overlap, resulting in in-plane (x and y direction) final vector spacing of approximately 0.3 mm. A post processing median filter and smoothing 3x3 kernel was applied once to resultant vector fields. All further post processing and computations were completed in Matlab.

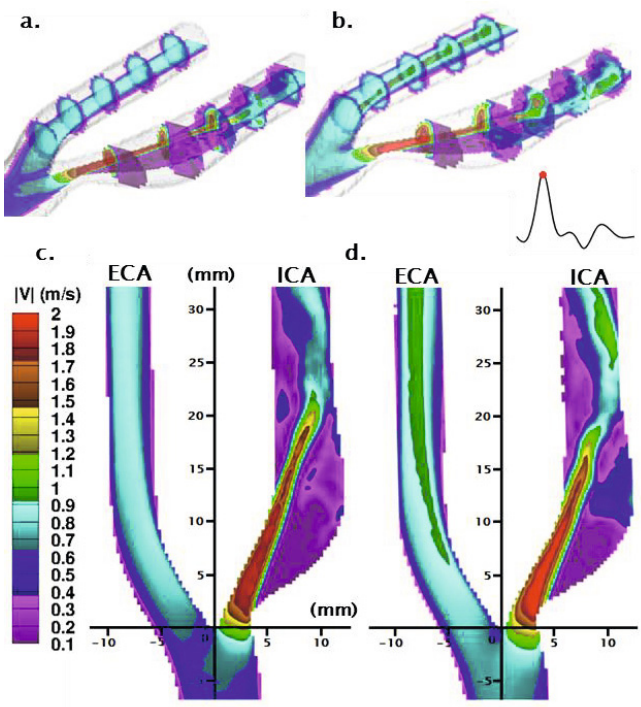

Fig. 1: Flow visualization at peak systole for thin vessel phantom model (a,c) and block phantom model (b,d). Central plane and cross-sectional slices of phase averaged velocity magnitude (spaced 6mm apart),are shown in top row (a,b). Central plane phase averaged velocity magnitude maps are shown in bottom row (c,d).

C. Turbulence Intensity Estimation

The turbulence intensity metric was used to quantify disturbed flow behaviour. Velocity maps were first ensemble averaged at each phase point based on the following:

$$V_i = \frac{1}{N}\sum_{n=0}^{N-1} v_i(t+nT), \qquad i = (x,y,z)$$

where N represents the number of total cardiac cycles (N=30) and T is the cycle period (T=920ms). Next, the phase-averaged flow was separated from non-coherent fluctuations using a Reynolds decomposition method [11]:

$$v_i'(t,n) = v_i(t,n) - V_i(t)$$

From these velocity fluctuations, the total turbulent intensity can be estimated as follows:

$$TI_{TOT}(t) = \sqrt{(TI_x(t))^2 + (TI_y(t))^2 + (TI_z(t))^2}$$

$$TI_i(t) = \sqrt{\frac{\sum_{n=1}^{N} v_i'(t,n)v_i'(t,n)}{N-1}}, \qquad i = x,y,z$$

A downstream region of interest (ROI), approximately 5 mm by 5 mm, was selected for each phantom over which an ROI averaged turbulence intensity value was calculated. The ROI was repositioned 5 times, up to 50% of ROI length upstream or downstream from the location of maximum turbulence, from which a mean ROI averaged TI value was calculated.

III. Results and Discussion

Figure 1 shows phase averaged velocity magnitude for both the thin vessel and block model at the time point corresponding to peak systole in their respective cardiac cycles. Note that the maximum CCA inlet velocity occurs 10 ms later for the thin vessel model compared to the rigid model as the compliance induces a phase delay. Higher velocities are observed overall in the block phantom, including slightly higher maximum jet velocities (1.98m/s) compared to the compliant model (1.90m/s). Both models exhibit a jet pattern in the ICA that begins at the stenosis throat, hugs the inner wall, crosses over and impinges on the outer wall. Two large recirculation zones exist on either side of the jet. Essentially laminar flow is observed in the ECA, as expected. A velocity vector map is shown for a cross-sectional slice located 12 mm distal to the apex in the ICA branch illustrating similar transverse flow patterns with a slight spiral forming in jet of the rigid model.

Figure 2 shows turbulence intensities in the ICA. Maximum turbulence intensity occurs where the jet dissipates during the deceleration phase following peak systole, as flow destabilizes. The rigid model shows a higher level of disturbed flow that also spans a broader area. Furthermore, this region of elevated turbulence intensity occurs more proximal/upstream in the rigid model, and notably where blood potentially feeds back into the large upstream recirculation zone. In vivo, platelets activated by high shear gradients are prone to preferentially adhere to the vessel wall in adjoining low shear regions. Thus increased turbulence in close proximity to the recirculation, as observed in the more rigid models, could lead to increased platelet aggregation and thrombus formation in these regions and also expose vulnerable plaques to highly disturbed flow.

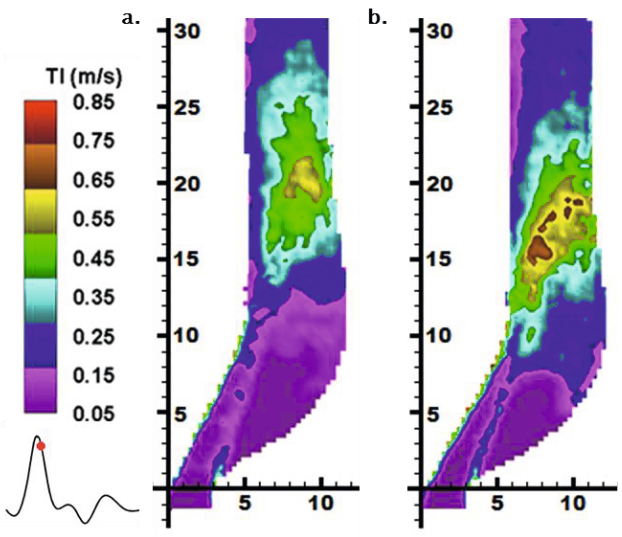

Fig. 2: Turbulence intensity maps in the ICA of the thin vessel model (a) and the block phantom model (b), for the time point following peak systole in each case.

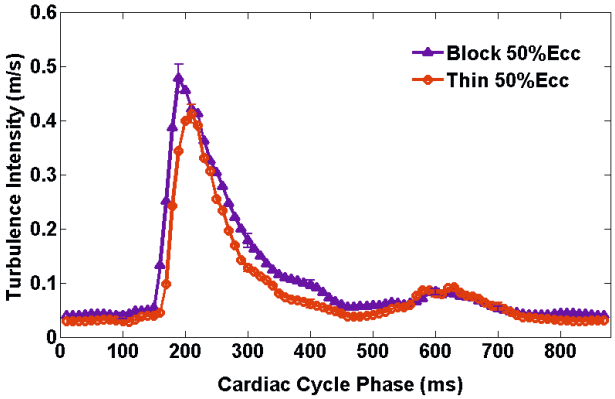

Fig. 3: Mean ROI averaged turbulence for block and thin vessel models plotte over cardiac cycle time.

Figure 3 shows the mean ROI averaged TI over time in the cardiac cycle. Peak values of 0.41±0.02 m/s in the thin phantom and 0.48±0.03 m/s in the block phantom were observed. It is also notable that the higher TI values in the rigid model drop off more slowly compared to the more compliant model.

The PDMS carotid models used here incorporate idealized geometry with highly planar symmetry, which imposes limitations on flow symmetry and elasticity/stiffness, but provide unique matched model family with controlled variables allowing the effect of only vessel compliance to be isolated.

IV. Conclusions

A matched model study was used to investigate the role of arterial compliance on the local hemodynamics in carotid artery phantoms with identical vessel geometry. It was observed that decreased compliance leads to higher velocities and higher levels of flow disturbance as quantified by the turbulence intensity metric.

Acknowledgment

The authors would like to acknowledge Hristo Nikolov for phantom fabrication, and Brian Dalrymple and Frank Van Sas for machining and technical expertise. Financial support is acknowledged from the Ontario Ministry of Research and Innovation (Early Researcher Award), Heart and

Stroke Foundation of Ontario (operating grant #T-6427), Natural Sciences and Engineering Research Council of Canada (Discovery Grant),

A.D. was partially supported by a Canadian Institutes of Health Research Training Fellowship in Vascular Research, a Canadian Institute of Health Sciences Banting and Best Master's Award, and the Ontario Graduate Scholarship program.

Conflict of Interest

The authors declare that they have no conflict of interest.

References

1. Cheng K S, Baker C R, Hamilton G et al. (2002) Arterial elastic properties and cardiovascular risk/event. Eur J Vasc Endovasc Surg 24:383-97
2. Dijk J M, van der Graaf Y, Grobbee D E et al. (2004) Carotid stiffness indicates risk of ischemic stroke and TIA in patients with internal carotid artery stenosis: the SMART study. Stroke 35:2258-62 DOI 10.1161/01.STR.0000141702.26898.e9
3. Groen H C, Gijsen F J, van der Lugt A et al. (2007) Plaque rupture in the carotid artery is localized at the high shear stress region: a case report. Stroke 38:2379-81 DOI 10.1161/STROKEAHA.107.484766
4. Hoi Y, Wasserman B A, Xie Y J et al. (2010) Characterization of volumetric flow rate waveforms at the carotid bifurcations of older adults. Physiol Meas 31:291-302 DOI 10.1088/0967-3334/31/3/002
5. Holdsworth D W, Rickey D W, Drangova M et al. (1991) Computer-controlled positive displacement pump for physiological flow simulation. Med Biol Eng Comput 29:565-70
6. Holdsworth D W, Norley C J, Frayne R et al. (1999) Characterization of common carotid artery blood-flow waveforms in normal human subjects. Physiol Meas 20:219-240
7. Kefayati S, Holdsworth D W and Poepping T L (2014) Turbulence intensity measurements using particle image velocimetry in diseased carotid artery models: effect of stenosis severity, plaque eccentricity, and ulceration. J Biomech 47:253-63 DOI 10.1016/j.jbiomech.2013.09.007
8. Kefayati S and Poepping T L (2013) Transitional flow analysis in the carotid artery bifurcation by proper orthogonal decomposition and particle image velocimetry. Med Eng Phys 35:898-909 DOI 10.1016/j.medengphy.2012.08.020
9. Laurent S, Katsahian S, Fassot C et al. (2003) Aortic stiffness is an independent predictor of fatal stroke in essential hypertension. Stroke 34:1203-6 DOI 10.1161/01.STR.0000065428.03209.64
10. Nesbitt W S, Westein E, Tovar-Lopez F J et al. (2009) A shear gradient-dependent platelet aggregation mechanism drives thrombus formation. Nat Med 15:665-73 DOI 10.1038/nm.1955
11. Poepping T L, Nikolov H N, Thorne M L et al. (2004) A thin-walled carotid vessel phantom for Doppler ultrasound flow studies. Ultrasound Med Biol 30:1067-78 DOI 10.1016/j.ultrasmedbio.2004.06.003
12. Reneman R S, van Merode T, Hick P et al. (1985) Flow velocity patterns in and distensibility of the carotid artery bulb in subjects of various ages. Circulation 71:500-9
13. Reynolds W C, Hussain A K M (1972) Mechanics of an organized wave in turbulent shear-flow: Theoretical Models and Comparison with Experiments. J Fluid Mech 54:263-8 DOI 10.1017/s0022112072000679
14. Smith R F, Rutt B K and Holdsworth D W (1999) Anthropomorphic carotid bifurcation phantom for MRI applications. J Magn Reson Imaging 10:533-44
15. Stein P D and Sabbah H N (1974) Measured turbulence and its effect on thrombus formation. Circ Res 35:608-14
16. Sugioka K, Hozumi T, Sciacca R R et al. (2002) Impact of aortic stiffness on ischemic stroke in elderly patients. Stroke 33:2077-81
17. Tsivgoulis G, Vemmos K, Papamichael C et al. (2006) Common carotid arterial stiffness and the risk of ischaemic stroke. Eur J Neurol 13:475-81 DOI 10.1111/j.1468-1331.2006.01291.x
18. van Popele N M, Grobbee D E, Bots M L et al. (2001) Association between arterial stiffness and atherosclerosis: the Rotterdam Study. Stroke 32:454-60
19. Vetel J, Garon A, Pelletier D (2009) Lagrangian coherent structures in the human carotid artery bifurcation. Exp Fluids 46:1067-1079 DOI 10.1007/s00348-009-0615-8
20. Yousif M Y, Holdsworth D W, Poepping T L (2011) A blood-mimicking fluid for particle image velocimetry with silicone vascular models. Exp Fluids 50:769-774 DOI 10.1007/s00348-010-0958-1
21. Zarins C K, Giddens D P, Bharadvaj B K et al. (1983) Carotid bifurcation atherosclerosis. Quantitative correlation of plaque localization with flow velocity profiles and wall shear stress. Circ Res 53:502-14